Journal of ELECTRONIC MATERIALS, Vol. 40, No. 5, 2011
DOI: 10.1007/s11664-011-1550-z

Granular and Lamellar Thermoelectric Oxides Consolidated by Spark Plasma Sintering

J.G. NOUDEM,[1,2] D. KENFAUI,[1] D. CHATEIGNER,[1] and M. GOMINA[1]

1.—Laboratoire CRISMAT, UMR 6508 ENSICAEN/CNRS, Université de Caen Basse-Normandie, 6 Boulevard Maréchal Juin, 14050 Caen Cedex 04, France. 2.—e-mail: jacques.noudem@ensicaen.fr

Using the spark plasma sintering (SPS) technique, dense nanostructured $Ca_{0.95}Sm_{0.05}MnO_3$ (*n*-type) and textured $Ca_3Co_4O_9$ (*p*-type) ceramics were prepared. Nanoceramic powders of doped *n*-type were synthesized using two routes: coprecipitation and solid-state reaction. The SPS method has been used to control the samples' densification and grain growth. Microstructural investigations reveal that the SPS technique results in high bulk density and homogeneous morphology for $Ca_{0.95}Sm_{0.05}MnO_3$, and grain alignment for $Ca_3Co_4O_9$. The thermoelectric and mechanical properties were investigated, showing a dependence on the starting grain size and being governed by the SPS conditions.

Key words: Oxides, $Ca_3Co_4O_9$, $CaSmMnO_3$, spark plasma sintering, thermoelectric, mechanical properties

INTRODUCTION

Discovering new *p*- and *n*-type thermoelectric (TE) phases or improving the TE properties of existing compounds[1–4] remains a challenge for the scientific community. To increase the electrical conductivity, reduce the thermal conductivity, and thereby improve the figure-of-merit *ZT*, alternative TE oxides have been suggested as potential candidates for high-temperature TE applications.[5–7]

The perovskite $CaMnO_3$ has been intensively studied[8–15] for its superconducting, magnetic, and electric properties, and the colossal magnetoresistance effect has been widely reported in this compound.[13,16,17] Dealing with TE properties, two approaches have been reported to modify the carrier concentration in order to enhance the material performance. The first approach is Ca-site substitution by La or Sm,[11,15,16,18] and the second approach is doping of Mn-sites with cations such as Nd, Ta, Ru, and Rh.[9,13,17] Various routes based on solution chemistry methods such as the nitrate method,[18,19] citrate gel with self-combustion,[10] and coprecipitation[20] have been used to prepare homogeneous and fine perovskite oxide powders. Whatever the synthesis method applied, TE performance still strongly depends on the densification and structuration from the nano- to the macroscale of the resulting samples.

The objective of this work is to investigate the spark plasma sintering process of nanostructured powders prepared by coprecipitation (nanoparticles synthesized by a chemical coprecipitation technique) and conventional microscopic powders (solid-state reaction). Results from microstructure analysis and thermal expansion measurements are compared with those obtained for samples prepared by using the conventional sintering method, and then correlated with the thermoelectric and mechanical properties. In addition, the correlation between the densification and texturation of lamellar $Ca_3Co_4O_9$ ceramics[21,22] by the SPS process, and the thermoelectric and mechanical properties is discussed.

Experimental Procedures

Two different electron-doped $Ca_{0.95}Sm_{0.05}MnO_3$ perovskite single-phase powders were prepared as previously described:[20] (1) nanocrystalline powder synthesized by a chemical coprecipitation technique,

(Received May 28, 2010; accepted January 24, 2011; published online March 11, 2011)

and (2) conventional crystalline powder obtained by the solid-state reaction method.

The samples were processed by using SPS (FCT Systems, Germany) using the following steps: In the first step, the powder was introduced into a graphite die (15 mm diameter), then placed into the working chamber under vacuum. A low pressure of 5 MPa was applied at the beginning of the sintering to insure a close loop for current injection through the graphite die. The temperature was increased up to the chosen sintering value in the 750°C to 900°C range at a rate of 100°C min^{-1}. Uniaxial pressure of 50 MPa was applied when the temperature reached 600°C, and released at the end of the dwell time (5 min). The sample was cooled to room temperature according to the thermal inertia of the furnace.

On the other hand, consolidation of the lamellar hole-doped $Ca_3Co_4O_9$ ceramics was investigated according to the experimental details described elsewhere.[23] The samples were prepared under 50 MPa at dwell temperatures of 750°C and 850°C for 2 min.

The density of the compacted samples was determined by using Archimedes' method (Kern & Sohn GmbH, Baligen, Germany), using deionized water as the liquid medium.

Phase identification was carried out by using an X'Pert powder diffractometer in Bragg–Brentano geometry. For $Ca_3Co_4O_9$ oxides, the texture was investigated using x-ray diffraction in a four-circle diffractometer setup equipped with a curved position-sensitive detector (CPS120; INEL, Artenay, France), and using monochromatized Cu K_α radiation, as described in detail elsewhere,[24] and within the combined analysis formalism[25] implemented in MAUD.[26]

Microstructural analysis was performed on fracture surfaces containing the pressing axis during processing, by using a Carl Zeiss (Supra 55; Oberkochen, Germany) scanning electron microscope (SEM) in backscattering electron (BSE) mode.

Bar-shaped samples of length 10 mm and cross-section 2 mm × 2 mm were cut from the processed samples by using a low-speed diamond saw (Struers, Champigny sur Marne, France), for physical characterization. The TE properties were measured (at steady state from 50°C to 800°C) by the direct-current (DC) four-probe method by using a ZEM-3 thermoelectric power and electrical resistivity measuring system (ULVAC-RIKO, Inc., Japan).

The mechanical properties (hardness, Young's modulus, flexural strength, and toughness) of $Ca_{0.95}Sm_{0.05}MnO_3$ and $Ca_3Co_4O_9$ ceramics were also determined. The microhardness, μH, was evaluated by carrying out Vickers indentation on mirror-polished surfaces of the samples by using a Zwick mechanical testing machine.

Instrumented nanoindentation tests were performed by using a XP Nano Indenter® (MTS Systems Corporation, Eden Prairie, MN) equipped with a Berkovich tip. For each test, impressions were introduced on the mirror-polished surface area of the samples parallel to the pressing axis. After the indentation load was removed, load–displacement (load–penetration depth) data were used to calculate the nanohardness, nH, and the elastic modulus (Young's modulus), E. Both properties were evaluated according to the formulae reported elsewhere.[23]

The strength, σ_R, of the ceramics was measured using three-point bending tests. The tested bars were cut from the different samples with almost the same dimensions: thickness $w \approx 2$ mm and width $B \approx 3$ mm. The span was set at 12 mm, and the load was applied parallel to the pressing axis. To measure the fracture toughness, K_{Ic}, single-edge notched beam (SNEB) specimens with relative notch length of $0.33w$ were prepared.

RESULTS AND DISCUSSION

The thermal expansion behavior of $Ca_{0.95}Sm_{0.05}MnO_3$ nanopowder prepared by coprecipitation and micron-particle-size powder obtained by solid-state reaction was investigated (Fig. 1). The experiments showed that the sintering behavior of the nanocrystalline sample was different from that of the micron-grain-size sample. Sintering of the latter to full density was not achieved up to 1450°C, while the former can occur in the solid phase at a lower temperature.

The shrinkage can be attributed to the densification mechanism, and can be faster for samples with smaller grain size. For both types of samples, the thermal expansion curves between room temperature and 1450°C can be sketched by considering two main zones: (1) from room temperature to ~900°C to 1000°C, one can observe a plateau corresponding only to thermal dilatation; and (2) shrinkage occurs at 900°C to 1000°C when sintering begins, and

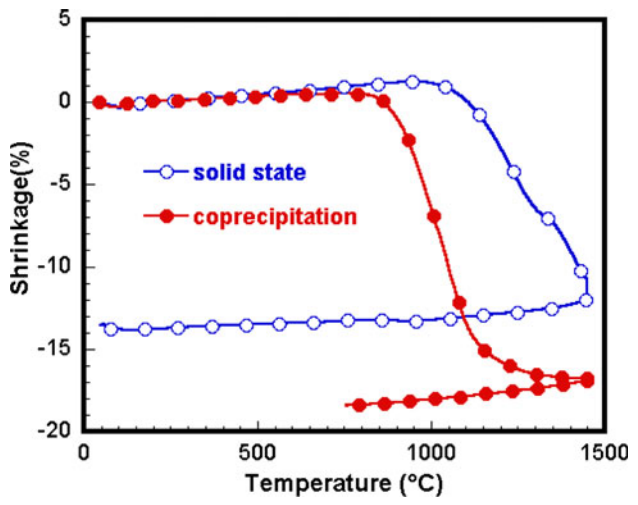

Fig. 1. Thermal expansion diagram of the compacted nanocrystalline and conventional $Ca_{0.95}Sm_{0.05}MnO_3$.

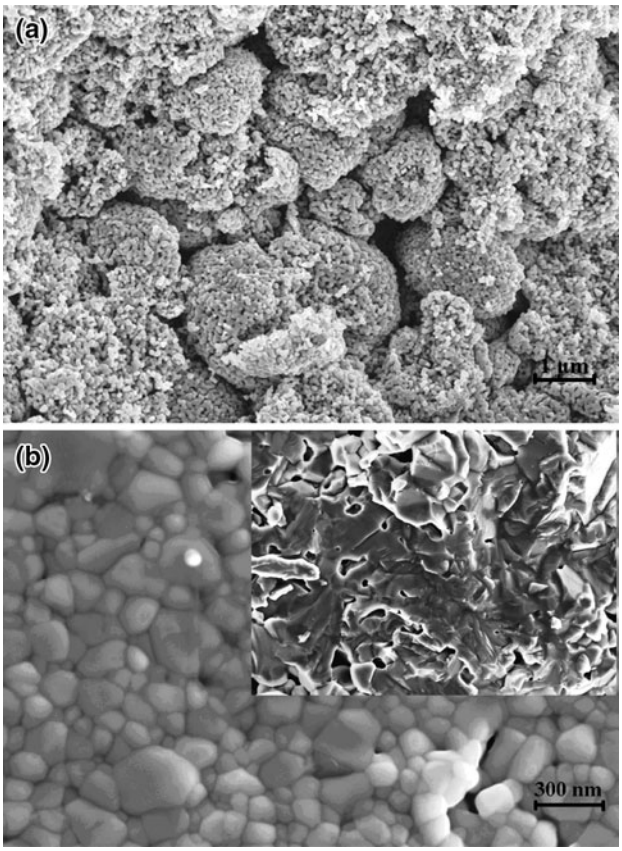

Fig. 2. SEM micrographs of (a) $Ca_{0.95}Sm_{0.05}MnO_3$ powder synthesized by coprecipitation method, and (b) sample consolidated by SPS from nanocrystalline powder and (inset) from micron-particle-size powder.

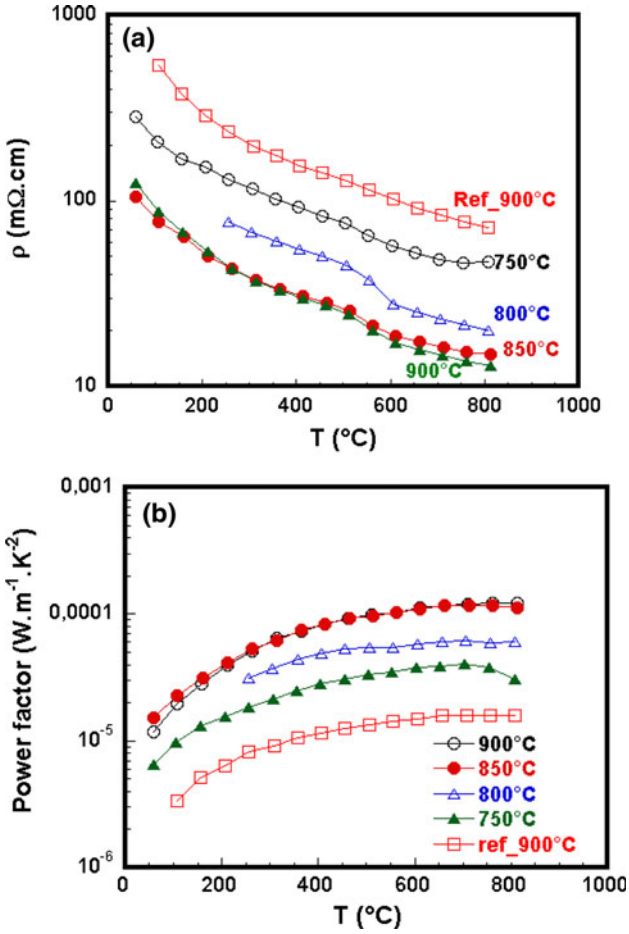

Fig. 3. Temperature dependence of (a) the electrical resistivity, and (b) the power factor for various processing temperatures.

continues up to 1450°C. The shrinkage amplitude is clearly related to the starting grain size, being 13% and 18% for micron-grain-size and nano-grain-size samples, respectively.

To investigate the phase development of nanopowders, the powder was calcined[20] in air for 6 h at various temperatures. The crystalline phase of $Ca_{0.95}Sm_{0.05}MnO_3$ was developed above 700°C, and the single phase formed at 900°C. The refined orthorhombic lattice parameters are a = 5.286(6) Å, b = 7.480(8) Å, and c = 5.272(5) Å with space group *Pnma*. Noticeable peak broadening is observed, indicating that the grain size is especially fine. A rough calculation using Scherrer equation[27] gives an average grain size of 60 nm to 70 nm, which correlates well with further SEM grain morphology observation.

Figure 2a shows SEM images of the ball-shaped nanopowder aggregates with sizes in the 2 μm to 3 μm range. In the present case, each ball is constituted of crystallites with dimensions of about 80 nm. As seen in Fig. 2b, the SPS process results in a homogeneous microstructure with narrow grain size distribution. Grain growth during the SPS process can be clearly observed. As expected, the sample consolidated from the solid-state reaction powder has larger grain size (inset of Fig. 2b) in comparison with the nanopowder. The bulk densities are 4.50 g cm^{-3} and 4.36 g cm^{-3} for the nano- and micron-particle-size samples, respectively, in agreement with the theoretical density of 4.59 g cm^{-3}.

Results of electrical resistivity (ρ) measurements are shown in Fig. 3a. For all the samples, the $\rho(T)$ curve shows semiconducting behavior, and resistivity decreases for higher SPS processing temperatures. Comparison of the two samples processed at 900°C clearly shows the difference in ρ values, probably due to the starting powder, densification, and grain connectivity. The temperature dependence of the Seebeck coefficient (S) of all samples seems characteristic of n-type TE materials over the whole measured temperature range. This n-type behavior indicates that electrons dominate the transport properties. The Seebeck coefficient decreases as the temperature is increased (-190 μV K^{-1} at 800°C). The power factors deduced from resistivity and Seebeck coefficient measurements are shown in Fig. 3b, where the influence of sample densification due to the processing

Table I. Mechanical properties of $Ca_{0.95}Sm_{0.05}MnO_3$ ceramics

Sample	μH (GPa)	nH (GPa)	E (GPa)	σ_R (MPa)	K_{Ic} (MPa $m^{1/2}$)
CS	1.25 ± 0.07	2.51 ± 0.31	100.78 ± 6.12	140.34 ± 5	–
SPS	8.51 ± 0.21	11.05 ± 0.6	205.2 ± 5.5	300 ± 15	4.99 ± 0.52

temperature is evidenced. The obtained values are comparable to results reported elsewhere.[9,11]

The average values of the mechanical properties obtained for $Ca_{0.95}Sm_{0.05}MnO_3$ ceramics consolidated by the conventional sintering (CS) and SPS processes are given in Table I.

The microhardness, μH, of the SPS sample (8.51 ± 0.21 GPa) is about 7 times larger than that of the CS sample. Such an improvement in μH may be related to the homogeneous nanostructure and essentially to the stronger densification (98.5%). The obtained value is also about 14 times larger than that reported for the conventional material Bi_2Te_3,[28] usually used in thermoelectric modules for energy conversion applications.

For the SPS sample, Vickers indentation generates microcracks around the corners of the indent. By measuring the crack lengths and using the formula reported elsewhere,[29] we estimated the fracture toughness, K_{Ic}, to be almost 5 ± 0.5 MPa $m^{1/2}$, which is larger than that reported for $Ca_3Co_4O_9$ ceramics,[23] a good p-type candidate for integration with $Ca_{0.95}Sm_{0.05}MnO_3$ materials in thermoelectric modules.

Due to similar factors found for μH, the nanohardness, nH, obtained for the SPS sample is reinforced by a factor of 4, compared with the CS sample. However, the nH of both CS and SPS ceramics displays an increase of 1.26 GPa and 2.54 GPa, respectively, compared with the μH values, corresponding to the more local character of nanoindentation measurement. This may indicate that nH values are closer to those of individual grains, while those of μH correspond to more macroscopic values taking into account grain boundaries and porosity effects.

Like the hardness, the elastic modulus, E, depends on the processing method. E was two times larger for ceramics consolidated by SPS and reached 205.2 ± 5.6 GPa. This value is about 6 and 2.5 times larger than those reported for Bi_2Te_3[30] and $Ca_3Co_4O_9$ ceramics,[23] respectively.

The results of three-point bending tests pointed out both the brittle behavior of $Ca_{0.95}Sm_{0.05}MnO_3$ ceramics and the effectiveness of the SPS process to enhance their strength, σ_R. An improvement in σ_R of more than twofold was recorded for the SPS sample (300.4 ± 14.6 GPa) compared with the CS sample (140.3 ± 5 GPa).

It should be noted also that the σ_R value of the SPS sample is 2.5 times larger than that found for Bi_2Te_3,[28] but comparable to that reported for $Ca_3Co_4O_9$ materials.[23]

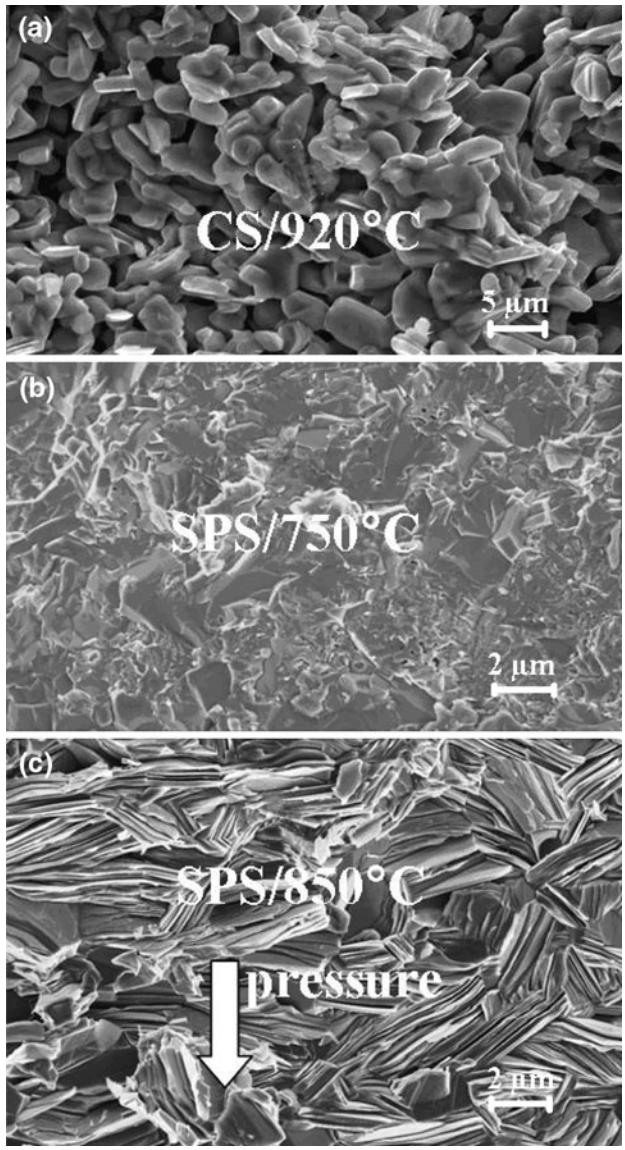

Fig. 4. Backscattering SEM microfractography of (a) the conventional sintered sample at 920°C, and SPS samples elaborated at (b) 750°C and (c) 850°C.

Figure 4 shows SEM images of the fracture surfaces of the $Ca_3Co_4O_9$ reference sample processed by CS without any applied pressure (0 MPa), and of the sample consolidated by the SPS process. The CS sample sintered at 920°C (Fig. 4a) exhibits underdeveloped grains with a porous microstructure compared with the well-compact and crystallized grains observed for the SPS sample elaborated at

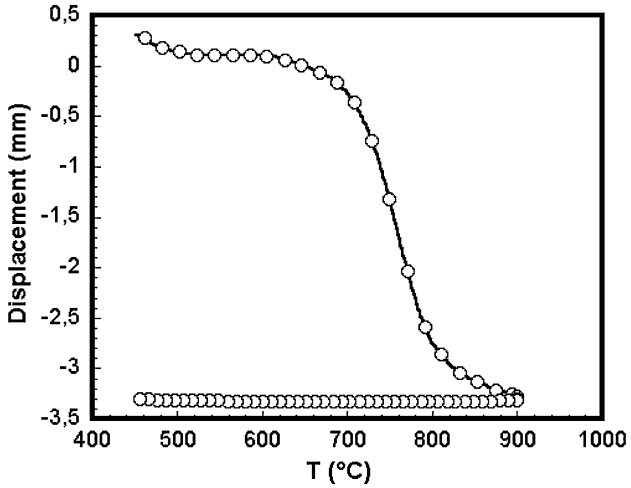

Fig. 5. Temperature dependence of the variation of the sample dimensions versus the temperature during SPS process.

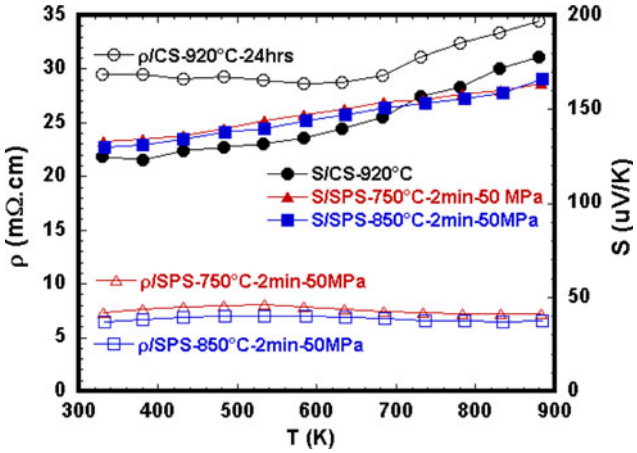

Fig. 7. Temperature dependence of electrical resistivity (open symbols) and Seebeck coefficient (filled symbols).

750°C (Fig. 4b). This is a useful advantage of the SPS process for the production of denser microstructure at lower temperature compared with the CS process. At an intermediate temperature of 850°C (Fig. 4c), the SPS sample shows very well-crystallized grains with relatively oriented zones. The bulk density of the samples are 3.1 g cm^{-3} (CS, 920°C), 4.45 g cm^{-3} (SPS, 750°C) and 4.57 g cm^{-3} (SPS, 850°C) corresponding to 57%, 95%, and 98%, respectively, of the theoretical density.[21] The densification of the SPS-processed sample is correlated to the temperature dependence of the shrinkage (Fig. 5) during SPS processing. Obviously, the powder is compacted from 450°C to 600°C, followed by densification and sintering associated with high shrinkage from 600°C to 900°C.

While the CS sample exhibited no crystallographic texture, results from quantitative texture analysis (combined analysis) of the samples processed by SPS reveal an increase of the texture strength when the dwell temperature applied during the processing was increased. Indeed, the maximum of {001} pole figures reached 2.15 mrd and 3.41 mrd at the center of {100} for the samples processed at 750°C and 580°C, respectively (Fig. 6). This indicates that the grains tend to be transformed into larger platelets and the ⟨001⟩* directions tend to be aligned parallel to the stress axis, notably for the sample sintered at high temperature, in agreement with the SEM observations. However, such texture levels remain much lower than those reported[23] for $Ca_3Co_4O_9$ ceramics elaborated by using the hot-pressing process.

The temperature dependence of the resistivity (ρ) and the thermoelectric power (S) from room temperature to 873 K was investigated (Fig. 7). The resistivity slope in this temperature range exhibits a different behavior between CS and SPS samples. While the behavior of the CS sample is clearly metallic above 600 K, and roughly semiconducting-like below, the SPS samples show opposite slopes in these temperature ranges. Since the CS sample is more porous, its behavior below 600 K is strongly linked to the porosity or intergranular medium, not related to the phase behavior. The observed transition at about 500 K has been reported to be probably related to either magnetic[31] or structural transformations.[32] The two SPS samples show the same resistivity behavior, but the resistivity values measured at room temperature are 8 mΩ cm and 6 mΩ cm for the SPS/750°C and SPS/850°C samples, respectively. These values are five times lower than the resistivity of the CS sample, for which

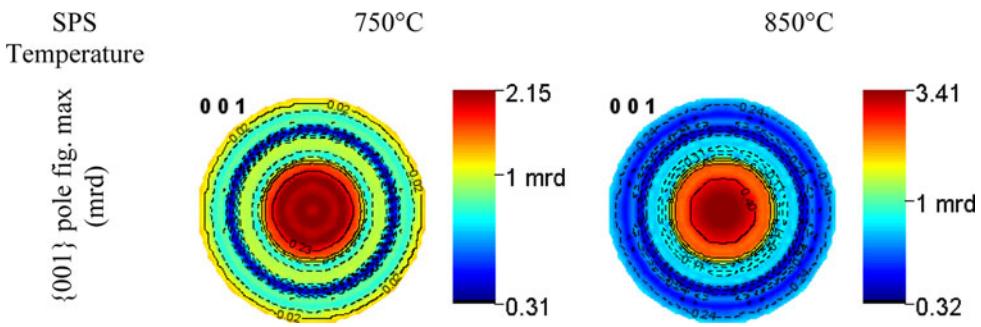

Fig. 6. Normalized {100} pole figures for the $Ca_3Co_4O_9$ samples processed by SPS at 750°C and 850°C.

Table II. Mechanical properties of $Ca_3Co_4O_9$ ceramics

Samples	μH (GPa)	nH (GPa)	E (GPa)	σ_R (MPa)	K_{Ic} (MPa $m^{1/2}$)
CS/920°C	0.12 ± 0.01	0.11 ± 0.03	10 ± 2	18.4 ± 2.5	0.39 ± 0.02
SPS/750°C	–	1.13 ± 0.43	23.35 ± 1.13	141 ± 8	0.70 ± 0.06
SPS/850°C	–	2.34 ± 0.15	66 ± 2.6	285 ± 6	1.95 ± 0.04

30 mΩ cm and 35 mΩ cm were measured at room temperature and at 873 K, respectively. This clearly shows that the resistivity has been decreased by increasing the sample density, inducing platelet alignment and promoting grain growth using the SPS technique. The slightly larger resistivity of the SPS sample elaborated at 750°C may be due to its slightly lower density.

The positive Seebeck coefficient S value is an indication[3,11,20] of the hole-mediated conduction in $Ca_3Co_4O_9$. The S values (Fig. 7) do not seem to depend on the microstructure, with similar behavior whatever the sintering process. For all samples, S increases with temperature and reaches 180 $\mu V\ K^{-1}$ at 873 K for CS. Such values are comparable to literature data.[22,27]

The temperature dependence of the resulting TE power factor S^2/ρ, for the CS and SPS samples is given in Fig. 7. At room temperature, power factor values of 88 $\mu W\ m^{-1}\ K^{-2}$ and 260 $\mu W\ m^{-1}\ K^{-2}$ were obtained for the CS and SPS (850°C) samples, respectively. These values increase with temperature up to 143 $\mu W\ m^{-1}\ K^{-2}$ and 422 $\mu W\ m^{-1}\ K^{-2}$ at 873 K, respectively. The SPS/750°C sample exhibits an intermediate power factor of 242 $\mu W\ m^{-1}\ K^{-2}$ and 375 $\mu W\ m^{-1}\ K^{-2}$ at room temperature and 873 K, respectively. The power factor values obtained for the SPS are comparable to the best reported values[22,33] values of the literature.

The mechanical properties determined for the $Ca_3Co_4O_9$ samples are given in Table II, which clearly shows that SPS is an effective way to improve these properties. The nanohardness, nH, the Young's modulus, E, strength, σ_R, and the fracture toughness, K_{Ic}, of the samples processed by SPS at 850°C are 21, 6.6, 15, and 2.16 times larger than those recorded for the CS samples. This improvement is essentially related to the strong densification as a consequence of the SPS process, but we should not forget the effect of texture and grain growth. The mechanical properties depend on the SPS processing parameters. Indeed, they increase significantly when the dwell temperature is increased.

The obtained value of σ_R is similar to that found for the nanostructured $Ca_{0.95}Sm_{0.05}MnO_3$ processed by SPS, but the values of nH, E, and K_{Ic} are lower.

CONCLUSIONS

Dense nanostructured $Ca_{0.95}Sm_{0.05}MnO_3$ thermoelectric ceramics have been obtained by combining coprecipitation synthesis with nonconventional SPS. The thermoelectric properties were investigated and compared with reported values.

Also, the SPS technique allows elaboration of highly dense $Ca_3Co_4O_9$ (98%) with uniform grain morphology at lower temperature and shorter sintering time. Compared with CS, the SPS sample exhibits a platelet-like orientation as evidenced by microstructure analysis. High bulk density, lower electrical resistivity, and enhanced thermoelectric power factor have been obtained.

The mechanical properties of $Ca_{0.95}Sm_{0.05}MnO_3$ and $Ca_3Co_4O_9$ ceramics are drastically improved by using the SPS process. For both materials, this improvement is essentially related to the densification, but also to the homogeneous microstructure for $Ca_{0.95}Sm_{0.05}MnO_3$, and to grain alignment and growth for $Ca_3Co_4O_9$. The obtained values are larger than those of the conventional TE material Bi_2Te_3.

Optimization of sintering parameters such as the maximum temperature, the dwell time, and the uniaxial pressure applied during processing is under investigation to control grain growth.

ACKNOWLEDGEMENTS

D. Kenfaui and the coauthors acknowledge the Conseil Régional de Basse Normandie, France for its PhD fellowship funding. The authors would like to acknowledge the Conseil Régional de Basse-Normandie, France and FEDER for financial participation in the experimental setup used in this work.

REFERENCES

1. L.D. Chen, T. Kawahara, X.F. Tang, T. Goto, J.S. Dyck, W. Chen, and C. Uher, *J. Appl. Phys.* 90, 1864 (2001).
2. N. Tohge, T. Minami, Y. Yamamoto, and M. Tanaka, *J. Appl. Phys.* 51, 1048 (1980).
3. I. Terasaki, Y. Sasago, and K. Uchinokura, *Phys. Rev. B* 56, R12685 (1997).
4. M. Hervieu, Ph. Boullay, C. Michel, A. Maignan, and B. Raveau, *J. Solid State Chem.* 142, 305 (1999).
5. M. Kazeoka, H. Hiramatsu, W.-S. Seo, and K. Koumoto, *J. Mater. Res.* 13, 523 (1998).
6. M. Ohtaki, T. Tsubata, K. Eguchi, and H. Arai, *J. Appl. Phys.* 79, 1816 (1996).
7. M. Ohtaki, D. Ogura, K. Eguchi, and H. Arai, *J. Mater. Chem.* 4, 653 (1994).
8. A. Maignan, C. Martin, F. Damay, B. Raveau, and J. Hejtmanek, *Phys. Rev. B* 58, 2758 (1998).
9. G. Xu, R. Funahashi, Q. Pu, B. Liu, R. Tao, G. Wang, and Z. Ding, *Solid State Ionics* 171, 147 (2004).

10. M.E. Melo Jorge, A. Carreia dos Santos, and M.R. Nunes, *Int. J. Inorg. Mater.* 3, 915 (2001).
11. M. Ohtaki, H. Koga, T. Tokutomu, K. Eguchi, and H. Arai, *J. Solid State Chem.* 120, 105 (1995).
12. A. Maignan, S. Hebert, L. Pi, D. Pelloquin, C. Martin, C. Michel, M. Hervieu, and B. Raveau, *Cryst. Eng.* 5, 365 (2002).
13. B. Raveau, Y.M. Zhao, C. Martin, M. Hervieu, and A. Maignan, *J. Solid State Chem.* 149, 203 (2000).
14. A.L. Cornelius, B.E. Light, and J.J. Neumeier, *Phys. Rev. B* 68, 014403 (2003).
15. T. Kobayashi, H. Takizawa, T. Endo, T. Sato, H. Taguchi, and M. Nagao, *J. Solid State Chem.* 92, 116 (1991).
16. A. Maignan, C. Martin, and B. Raveau, *Mater. Res. Bull.* 34, 345 (1999).
17. B. Raveau, A. Maignan, C. Martin, and M. Hervieu, *Mater. Res. Bull.* 35, 1579 (2000).
18. M.E. Melo Jorge, M.R. Nunes, R. Silvia Maria, and D. Sousa, *Chem. Mater.* 17, 2069 (2005).
19. J. Briatico, B. Alascio, R. Allub, A. Butera, A. Caneiro, M.T. Causa, and M. Tovar, *Phys. Rev. B* 53, 14020 (1996).
20. C.S. Sanmathi, R. Retoux, M.P. Singh, and J. Noudem, *Mater. Chem. Phys.* 114, 676 (2009).
21. A.C. Masset, C. Michel, A. Maignan, M. Hervieu, O. Toulemonde, F. Studer, B. Raveau, and J. Hejtmanek, *Phys. Rev. B* 62, 166 (2000).
22. M. Prevel, S. Lemonnier, Y. Klein, S. Hébert, D. Chateigner, B. Ouladdiaf, and J.G. Noudem, *J. Appl. Phys.* 98, 093706 (2005).
23. D. Kenfaui, D. Chateigner, M. Gomina, and J.G. Noudem, *J. Alloys Compd.* 490, 472 (2010).
24. J. Ricote and D. Chateigner, *Bol. Soc. Esp. Ceram. Vidrio* 38, 587 (1999).
25. D. Chateigner, ed., *Combined Analysis* (ISTE–Wiley, 2010), p. 496.
26. L. Lutterotti, S. Matthies, and H.R. Wenk, *Texture of Materials: Proceeding of ICOTOM14*, ed. J.A. Spunar (Ottawa: National Research Council of Canada, 1999), pp. 1599–1604.
27. A.L. Patterson, *Phys. Rev.* 56, 978 (1939).
28. L.-D. Zhao, B.-P. Zhang, J.-F. Li, M. Zhou, W.-S. Liu, and J. Liu, *J. Alloys Compd.* 455, 259 (2008).
29. F. Tancret, I. Monot, and F. Osterstock, *Mater. Sci. Eng. A* 298, 268 (2001).
30. Y. Zhou, I. Matsubara, R. Funahashi, G. Xu, and M. Shikano, *Mater. Res. Bull.* 38, 341 (2003).
31. P. Limelette, V. Hardy, P. Auban-Senzier, D. Jerôme, D. Flahaut, S. Hébert, R. Frésard, Ch. Simon, J. Noudem, and A. Maignan, *Phys. Rev. B* 71, 233108 (2005).
32. H. Muguera and D. Grebille, *Acta Crystallogr. B* 64, 676 (2008).
33. Y. Liu, Y. Lin, Z. Shi, C.-W. Nan, and Z. Shen, *J. Am. Ceram. Soc.* 88, 1337 (2005).